Human Brain Mapping

WILEY

TECHNICAL REPORT OPEN ACCESS

Revisiting Amplitude of Low-Frequency Fluctuations (ALFF) in Resting-State fMRI: Clarifications and Improvements

Lejian Huang[1,2] | Rami Jabakhanji[1,2] | Andrew D. Vigotsky[3] | Paulo Branco[2,4] | Marwan N. Baliki[2,5,6] | A. Vania Apkarian[1,2,4]

[1]Department of Neuroscience, Feinberg School of Medicine, Northwestern University, Chicago, Illinois, USA | [2]Center for Translational Pain Research, Feinberg School of Medicine, Northwestern University, Chicago, Illinois, USA | [3]Departments of Biomedical Engineering and Statistics and Data Science, Northwestern University, Evanston, Illinois, USA | [4]Department of Anesthesiology, Feinberg School of Medicine, Northwestern University, Chicago, Illinois, USA | [5]Department of Physical Medicine and Rehabilitation, Northwestern University, Chicago, Illinois, USA | [6]Shirley Ryan AbilityLab, Chicago, Illinois, USA

Correspondence: Lejian Huang (lejian-huang@northwestern.edu) | A. Vania Apkarian (a-apkarian@northwestern.edu)

Received: 11 September 2025 | **Revised:** 18 December 2025 | **Accepted:** 7 March 2026

Keywords: BOLD intensity | fMRI | qmALFF | qmfALFF | spontaneous neural activity | z-scoring

ABSTRACT

The amplitude of low-frequency fluctuations (ALFF) and its related measure, fractional ALFF (fALFF), are widely used resting-state fMRI techniques for quantifying spontaneous neural activity within specific frequency bands. However, inconsistencies in the definition and implementation of ALFF have led to confusion in the field. In this study, we provide a mathematical clarification of ALFF and fALFF by introducing two variants: the arithmetic mean-defined ALFF/fALFF (amALFF/amfALFF) and the quadratic mean-defined ALFF/fALFF (qmALFF/qmfALFF). We examine the relationships between mean BOLD intensity (MBI), amALFF, and qmALFF across both subjects and voxels using two independent datasets mapped onto different brain templates. Additionally, we investigate the impact of *z*-scoring the original BOLD signal on ALFF and fALFF metrics. Finally, we evaluate the validity and test–retest reliability of (f)ALFF using a dataset with two runs at voxel, parcellation, and cortical level. Our key findings include: (1) MBI is positively correlated with both amALFF and qmALFF, highlighting the need for normalization to subject-level means; (2) normalized qmALFF and qmfALFF are highly correlated with normalized amALFF and amfALFF, respectively, at both the subject and voxel levels; (3) *z*-scoring the BOLD signal does not affect amfALFF or qmfALFF, but it substantially alters amALFF and qmALFF; (4) ALFF exhibits higher reliability than fALFF and both perform best at the parcellation level compared to voxel and cortical (subject) levels. Based on these findings, we present a comprehensive flowchart of the (f)ALFF algorithm implemented in the temporal domain. The full procedure is implemented in R, and the corresponding script is available at: https://github.com/lejianhuang/ALFF.

1 | Introduction

The amplitude of low-frequency fluctuations (ALFF) and its closely related measure, fractional amplitude of low-frequency fluctuations (fALFF), are two widely used resting-state fMRI analysis techniques for quantifying the "amount" of spontaneous neural activity within a specific frequency range (Biswal et al. 1995; Zang et al. 2007; Zou et al. 2008). These measures have been extensively applied to investigate brain activity in various clinical conditions (Zang et al. 2007; Li et al. 2021; Sun et al. 2022; Mieling et al. 2023; Cattarinussi et al. 2025; Liu et al. 2025; Zhang et al. 2025), alongside

numerous methodological advancements (Chang et al. 2025; Liang et al. 2025).

Despite their extensive use, inconsistencies in the definition and implementation of ALFF have led to the conflation of distinct mathematical constructs within the neuroimaging literature. First, the original description of ALFF is unclear, that is, the average squared root of power instead of amplitude itself in the frequency domain (Zang et al. 2007). Although the authors directly link ALFF to amplitude in their updated software (Jia et al. 2019), the ambiguity from (Zang et al. 2007) has led to misrepresentation and errors in (Zuo et al. 2010; FCP-INDI 2024), which erroneously define ALFF as the total power (sum of squared amplitudes) within a specified bandwidth. Second, variations in methodological implementations have also contributed to the conflation within the literature (Song et al. 2011; Whitfield-Gabrieli and Nieto-Castanon 2012; Xu et al. 2018; Jia et al. 2019). For instance, in one commonly used ALFF toolbox, RESTplus (Song et al. 2011; Jia et al. 2019), ALFF is computed as the arithmetic mean of the power spectrum within a given frequency range. In contrast, another popular software, CONN (Whitfield-Gabrieli and Nieto-Castanon 2012), indirectly defines ALFF using the quadratic mean of the amplitude. In another toolbox, BRANT (Xu et al. 2018), while its related article defines ALFF as the average square root of the power spectral density, its implementation is the same as REST (Song et al. 2011) (the original version of RESTplus): the average square root of the power spectrum. These discrepancies are not merely theoretical—they can influence the magnitude and range of ALFF values, which in turn affects statistical comparisons and interpretation. For instance, implementations based on the sum of amplitudes are highly sensitive to acquisition parameters such as scan length and repetition time, introducing variability unrelated to neural activity (Yan et al. 2013). Additionally, preprocessing steps such as z-scoring the original BOLD signal, commonly applied for connectivity analyses, have not been systematically evaluated for their impact on ALFF and fALFF (Handwerker et al. 2012; Mohanty et al. 2020; Nieto-Castanon 2020). Given these inconsistencies and their potential to affect reproducibility and validity, it is imperative to rigorously revisit the definitions and computational procedures of ALFF and fALFF.

In this paper, we mathematically clarify ALFF and fALFF in terms of the arithmetic mean (amALFF/amfALFF) and the quadratic mean (qmALFF/qmfALFF). We also reexamine the relationships between mean BOLD intensity, amALFF, amfALFF, qmALFF, and qmfALFF at both subject and voxel levels across two independent datasets on two different brain templates. In addition, we show how z-scoring the original BOLD signal affects ALFF and fALFF. Finally, we evaluate the validity and reliability of qm(f)ALFF using an independent dataset. Based on our findings, we present a flowchart illustrating the complete (f)ALFF algorithm implemented in the temporal domain.

The amALFF and qmALFF proposed in this study do not introduce new mathematical operations beyond the arithmetic mean and quadratic mean; rather, they explicitly formalize these definitions to clarify the ambiguity in previous implementations. By explicitly naming and formalizing these two variants, we provide a clear mathematical framework. This clarification ensures transparency and reproducibility, which were lacking in prior implementations.

2 | Methods

2.1 | Arithmetic Mean of ALFF

Let $s(m, n)$ represent the preprocessed BOLD time-series signal of a voxel m at coordinates (x, y, z) in the brain after demeaning, where $m = (1, 2, ..., M)$ and $n = (0, 1, ..., N-1)$. Here, M and N denote the number of voxels masked by a given brain template and volumes (time points) of the resting-state (RS) fMRI data, respectively. Let $s_{bp}(m, n)$ denote the BOLD signal after applying a bandpass temporal filter. In this study, we used a zero-lag fourth-order Butterworth filter with a frequency band of 0.01–0.08 Hz. For simplicity, voxel coordinates will be omitted in the following descriptions.

The amplitude spectrum of $s(m, n)$ can be computed using the fast Fourier transform (FFT). The amplitude spectrum of $s(m, n)$ before scaling is given by

$$S(m,k) = \mid \mathrm{fft}(s(m,n)) \mid$$

where $k = (0, 1, ..., N-1)$ and the frequency interval between consecutive k-values is $\frac{1}{N \times \mathrm{TR}}$ Hz. TR (repetition time) represents the time interval between consecutive volume acquisitions in the RS-fMRI scan. For simplicity, and without loss of generality, we assume the number of sampling points, N, is even. The notation $|\cdot|$ represents the magnitude of each frequency component, computed as the square root of the sum of the squares of its real and imaginary parts after applying the FFT. $S(m, k)$, where $k = (1, 2, ..., N-1)$, is symmetric around $k = N/2$.

Thus, the arithmetic mean of ALFF (amALFF) for a given voxel m within a specified frequency range $[f_l, f_h]$ can be computed as

$$\mathrm{amALFF}(m) = \frac{1}{k_{f_h} - k_{f_l} + 1} \sum_{k=k_{f_l}}^{k_{f_h}} \frac{2S(m,k)}{N}, \tag{1}$$

where f_l and f_h represent the lowest and highest frequencies in the specified range (set to 0.01 Hz and 0.08 Hz in this study), and k_{f_h} and k_{f_l} denote the FFT indices corresponding to or closest to f_l and f_h, respectively. N is a scaling factor for normalization. This arithmetic mean of ALFF is consistent with the original definition and its derivative used for measuring ALFF in (Zang et al. 2007).

The arithmetic-mean fractional amplitude of low-frequency fluctuation (amfALFF) is defined as the ratio of the sum of amplitude spectrum within a specified frequency range $[f_l, f_h]$ to that of the frequency range $[0, f_c]$

$$\mathrm{amfALFF}(m) = \frac{\sum_{k=k_{f_l}}^{k_{f_h}} S(m,k)}{\sum_{k=0}^{k_{f_c}} S(m,k)}, \tag{2}$$

where f_c represents the low-pass cut-off frequency in the preprocessing stage (set to 0.2 Hz in this study), and k_{f_c} denotes the FFT index corresponding to or closest to f_c.

2.2 | Quadratic Mean of ALFF

The BOLD signal is an indirect measure of neuronal activity through hemodynamic responses. The mean power of $s(m, n)$ represents the average energy of consumption per unit time for a voxel m and is calculated as follows:

$$\frac{\sum_{k=0}^{N-1} S^2(m,k)}{N^2}$$

Accordingly, the mean power of $s(m, n)$ within a specified frequency range $[f_l, f_h]$ is given by

$$\frac{4}{N\left(k_{f_h} - k_{f_l} + 1\right)} \sum_{k=k_{f_l}}^{k_{f_h}} S^2(m,k)$$

The corresponding mean amplitude, defined as the quadratic mean of ALFF (qmALFF)

$$\mathrm{qmALFF}(m) = 2\sqrt{\frac{1}{N(k_{f_h} - k_{f_l} + 1)} \sum_{k=k_{f_l}}^{k_{f_h}} S^2(m,k)}$$

which can also be expressed as

$$\mathrm{qmALFF}(m) = 2\sqrt{\frac{N}{k_{f_h} - k_{f_l} + 1} \sum_{k=k_{f_l}}^{k_{f_h}} \left(\frac{S(m,k)}{N}\right)^2} \tag{3}$$

and similarly, the quadratic-mean fractional amplitude of low-frequency fluctuation (qmfALFF) can be given by

$$\mathrm{qmfALFF}(m) = \frac{\sqrt{\sum_{k=k_{f_l}}^{k_{f_h}} S^2(m,k)}}{\sqrt{\sum_{k=0}^{k_{f_c}} S^2(m,k)}} \tag{4}$$

Based on Parseval's Theorem, Equation (3) can be rewritten in the form of time domain as

$$\mathrm{qmALFF}(m) = 2\sqrt{\frac{N}{k_{f_h} - k_{f_l} + 1}}\, \mathrm{RMS}\left\{ s_{bp}(m,n)\,|_{(f_l,\ f_h)} \right\}, \tag{5}$$

where $\mathrm{RMS}\left\{ s_{bp}(m,n)\,|_{(f_l, f_h)} \right\}$ denotes the root mean square of $s(m, n)$ filtered by a bandpass filter with cutoff frequencies f_l and f_h. Thus, the qmfALFF in the form of time domain is given by

$$\mathrm{qmfALFF}(m) = \frac{\mathrm{RMS}\left\{ s_{bp}(m,n)\,|_{(f_l, f_h)} \right\}}{\mathrm{RMS}\{s(m,n)\}} \tag{6}$$

Note that $s(m, n)$ has been filtered by a low-pass temporal filter with the low-pass cut-off frequency f_c in the preprocessing stage.

2.3 | Correlations Between Mean BOLD Intensity and am/qm(f)ALFF

From Equations (1) and (3), both amALFF and qmALFF across voxels are influenced by the number of volumes and sampling points (N); repetition time(TR), which determines FFT index (k_{f_h} and k_{f_l}) based on f_l and f_h; and the mean BOLD intensity (MBI) across time series through $S(m, k)$, even though $s(m, n)$ is demeaned before calculating am/qmALFF. In a given study, TR and N remain constant once the study protocol is set. However, the MBI may vary due to several factors, such as scanner settings, participant physiology, and preprocessing steps (Huang et al. 2012; Krishnamurthy et al. 2020). Therefore, it is essential to examine the correlations between MBI and am/qm(f)ALFF at both subject (mean of MBI across voxels) and voxel levels (MBI of voxel). Salient correlations that exist between these variables should be addressed before proceeding with further analyses. At subject level, the MBI is calculated as the mean of MBI across voxels within a given template in brain. At voxel level, the MBI is calculated as the mean of MBI across subjects for each voxel within a given template in a brain.

2.4 | Normalization of am/qmALFF at the Subject Level

If a salient correlation exists between MBI and am/qm ALFF across subjects, it is reasonable to normalize the am/qm ALFF value to ensure the mean am/qm ALFF for each subject equals 1. This normalization minimizes inter-subject variability that is attributable to MBI and ensures comparability across individuals.

The normalized amALFF, denoted as $\mathrm{amALFF}_{\mathrm{norm}}$, for the voxel m is calculated as follows:

$$\mathrm{amALFF}_{\mathrm{norm}}(m) = \frac{\sum_{k=k_{f_l}}^{k_{f_h}} S(m,k)}{\frac{1}{M}\sum_{m=1}^{M}\sum_{k=k_{f_l}}^{k_{f_h}} S(m,k)} \tag{7}$$

Equation (7) shows that the final analysis results in studies relying on the original version of ALFF (incorrectly defined as $\sum_{k=k_{f_l}}^{k_{f_h}} S(m,k)$) will not be affected if amALFF is normalized. The normalization allows the factors in Equation (1) to be canceled out from the numerator and denominator of the Equation (7).

Similarly, the normalized qmALFF, $\mathrm{qmALFF}_{\mathrm{norm}}$, is defined as.

$$\mathrm{qmALFF}_{\mathrm{norm}}(m) = \frac{\sqrt{\sum_{k=k_{f_l}}^{k_{f_h}} S^2(m,k)}}{\frac{1}{M}\sum_{m=1}^{M}\sqrt{\sum_{k=k_{f_l}}^{k_{f_h}} S^2(m,k)}} \tag{8}$$

or

$$\mathrm{qmALFF}_{\mathrm{norm}}(m) = \frac{\mathrm{RMS}\left\{ s_{bp}(m,n)\,|_{(f_l,\ f_h)} \right\}}{\frac{1}{M}\sum_{m=1}^{M} \mathrm{RMS}\left\{ s_{bp}(m,n)\,|_{(f_l,\ f_h)} \right\}} \tag{9}$$

2.5 | The Effect of *z*-Scoring on am/qm fALFF and am/qmALFF$_{\mathrm{norm}}$

z-scoring the BOLD signal over time does not alter the relative frequency content or the overall spectral shape. Instead, it scales the entire amplitude spectrum by a constant factor and removes the zero-frequency (demean). Mathematically, the *z*-scored amplitude spectrum is given by

$$S_z(m,k) = \frac{S(m,k)}{\sigma(m)}$$

where $\sigma(m)$ denotes the standard deviation of $s(m,\ n)$, and $S_z(m,k)$ is the amplitude spectrum of the *z*-scored signal $s(m,n)$. From Equations (2) and (4), it follows that *z*-scoring does not affect amfALFF or qmfALFF, since $\sigma(m)$ in each equation can be canceled out from the numerator and denominator. Moreover, according to Equation (6), when $s(m,\ n)$ is *z*-scored, such that $\mathrm{RMS}\{s(m,n)\} = 1$, qmALFF becomes.

$$\mathrm{qmfALFF}(m) = \mathrm{RMS}\left\{ s_{bp,z}(m,n)\,|_{(f_l,\ f_h)} \right\}, \tag{10}$$

where $\mathrm{RMS}\left\{ s_{bp,z}(m,n)\,|_{(f_l f_h)} \right\}$ represents the root mean square of *z*-scored signal $s(m,\ n)$, filtered using a bandpass filter with cutoff frequencies f_l and f_h.

By *z*-scoring the normalized metrics, amALFF$_{\mathrm{norm}}$ and qmALFF$_{\mathrm{norm}}$, we obtain

$$\mathrm{amALFF}_{\mathrm{norm},z}(m) = \frac{\frac{1}{\sigma(m)}\sum_{k=k_{f_l}}^{k_{f_h}} S(m,k)}{\frac{1}{M}\sum_{m=1}^{M}\left(\frac{1}{\sigma(m)}\sum_{k=k_{f_l}}^{k_{f_h}} S(m,k)\right)} \tag{11}$$

and

$$\mathrm{qmALFF}_{\mathrm{norm},z}(m) = \frac{\frac{1}{\sigma(m)}\sqrt{\sum_{k=k_{f_l}}^{k_{f_h}} S^2(m,k)}}{\frac{1}{M}\sum_{m=1}^{M}\left(\frac{1}{\sigma(m)}\sqrt{\sum_{k=k_{f_l}}^{k_{f_h}} S^2(m,k)}\right)} \tag{12}$$

These expressions indicate that amALFF$_{\mathrm{norm}}$ and qmALFF$_{\mathrm{norm}}$ are equal to their *z*-scored counterparts (amALFF$_{\mathrm{norm},z}$ and qmALFF$_{\mathrm{norm},z}$) if and only if $\sigma(1) = \sigma(2) = \ \ldots\ = \sigma(M)$.

2.6 | Validation and Reliability of Qm(f)ALFF

The metrics amALFF and amfALFF have been extensively validated and widely used to quantify spontaneous neural activity, with applications in healthy populations and various clinical conditions (Cordes et al. 2001; Yang et al. 2007, 2018; Lencz et al. 2022; Montalà-Flaquer et al. 2023; Cattarinussi et al. 2025). In this study, to validate qm(f)ALFF, we computed Pearson correlations between qm(f)ALFF (or qm(f)ALFF$_{\mathrm{norm}}$) and am(f)ALFF (or am(f)ALFF$_{\mathrm{norm}}$) in the NU26 dataset at voxel, parcellation, and cortical levels.

At the voxel and parcellation level, for each subject, correlations are calculated between qmALFF$_{\mathrm{norm}}$ and amALFF$_{\mathrm{norm}}$ and between qmfALFF and amfALFF across voxels or parcellations within the Schaefer cortical template (Schaefer et al. 2018). At the cortical level, correlations are calculated between mean qm(f)ALFF and mean am(f)ALFF across subjects using the Schaefer cortical template.

Reliability of qm(f)ALFF was assessed using the Intraclass Correlation Coefficient (ICC) (Bartko 1966), which measures the consistency between two RS-fMRI scans for each subject at voxel, parcellation, and cortical levels. ICC values were calculated using the ***icc*** function with a one-way model from the ***irr*** package in R (version 4.4.0).

2.7 | Datasets

This study utilizes three datasets. The first dataset, from a previous study in China, includes 167 healthy controls in (Yang et al. 2022) (China167) (83 males, 84 females; mean age ± SD: 41 ± 14 years old).

The second dataset comes from the Human Connectome Project 1200 (HCP1200) (Van Essen et al. 2013), which includes 926 young healthy volunteers after quality control (425 males, 501 females; mean age m ± SD: 29 ± 4 years old). We found that the HCP1200 dataset has three clusters of MBI (subjects with low (*l*), medium (*m*), and high (*h*) MBI are 14, 759, and 153, respectively).

The third dataset is from an ongoing study at Northwestern University (NU26) and includes 26 healthy volunteers (10 males, 16 females; mean age ± SD: 65 ± 8 years old). Each participant underwent two RS-fMRI scans. This dataset is used to assess the validation and reliability of qm(f)ALFF.

2.8 | MRI Scanning Parameters

For the China167 dataset, subjects were scanned on a 3 Tesla GE-Discovery 750. T1 images were acquired with following parameters: voxel size = 1 × 1 × 1 mm^3; TR/TE = 7.7/3.4 ms; flip angle = 12°; field of view = 256 × 256 mm^2. RS-fMRI images were acquired with the following parameters: voxel size = 3.43 75 × 3.4375 × 3.5 mm^3; TR/TE = 2500/30 ms; flip angle = 90°; in-plane resolution = 64 × 64; field of view = 220 × 220 mm^2; number of volumes = 230; slices per volume = 42, which covers the whole brain from the cerebellum to the vertex.

For the HCP1200 dataset, subjects were scanned on a 3 Tesla GE-Discovery 750. T1 images were acquired with following parameters: voxel size = 0.7 × 0.7 × 0.7 mm^3; TR/TE = 2400/2.14 ms; flip angle = 8°; field of view = 224 × 224 mm^2.

RS-fMRI images were acquired with the following parameters: voxel size = 2 × 2 × 2 mm^3; TR/TE = 720/33.1 ms; flip angle = 52°; field of view = 208 × 180 mm^2; number of volumes = 1200; multiband accelerator = 8; slices per volume = 72, which covers the whole brain from the cerebellum to the vertex.

For the NU26 dataset, subjects were scanned on a clinical 3 Tesla Siemens Magnetom Prisma whole body scanner equipped with a 64 channel-head/neck coil. T1 images were acquired with following parameters: voxel size = 1 × 1 × 1 mm^3; TR/TE = 2.3 s/2.40 ms; flip angle = 9°; field of view = 256 × 256 mm^2. RS-fMRI images were acquired with the following parameters: voxel size = 2 × 2 × 2 mm^3; TR/TE = 555/22 ms; flip angle = 47°; in-plane resolution = 96 × 104; number of volumes = 1110; multiband accelerator = 8; slices per volume = 64 acquired with interleaved ordering, which covers the whole brain from the cerebellum to the vertex.

2.9 | RS-fMRI Data Preprocessing and Denoising

Both datasets were preprocessed using fmriprep version 23.1.4 (Esteban et al. 2019), a Nipype-based tool (Gorgolewski et al. 2011, 2017). Each T1w (T1-weighted) volume was skull-stripped using antsBrainExtraction.sh v2.1.0 (using the OASIS NKI template). Brain surfaces were reconstructed using recon-all from FreeSurfer v6.0.1 (Dale et al. 1999), and the brain mask estimated previously was refined with a custom variation of the method to reconcile ANTs-derived and FreeSurfer-derived segmentations of the cortical gray-matter of Mindboggle (Klein et al. 2017). Spatial normalization to the ICBM 152 Nonlinear Asymmetrical template version 2009c (Fonov et al. 2009) was performed through nonlinear registration with the antsRegistration tool of ANTs v2.1.0 (Avants et al. 2008), using brain-extracted versions of both T1w volume and template. Brain tissue segmentation of cerebrospinal fluid (CSF), white-matter (WM), and gray-matter (GM) was performed on the brain-extracted T1w using fast (Zhang et al. 2001).

Functional data was slice time corrected using 3dTshift from AFNI v16.2.07 (Cox 1996) and motion corrected using mcflirt (Jenkinson et al. 2002). No distortion correction was performed. This was followed by co-registration to the corresponding T1w using boundary-based registration (Greve and Fischl 2009) with six degrees of freedom, using bbregister (FreeSurfer v6.0.1). flirt (FSL). Motion correcting transformations and BOLD-to-T1w transformation and T1w-to-template (MNI) warp were concatenated and applied in a single step using antsApplyTransforms (ANTs v2.1.0) using Lanczos interpolation.

Physiological noise regressors were extracted applying CompCor (Behzadi et al. 2007). Principal components were estimated for the two CompCor variants: temporal (tCompCor) and anatomical (aCompCor). A mask to exclude signal with cortical origin was obtained by eroding the brain mask, ensuring it only contained subcortical structures. Six tCompCor components were then calculated, including only the top 5% variable voxels within that subcortical mask. For aCompCor, six components were calculated within the intersection of the subcortical mask and the union of CSF and WM masks calculated in T1w space, after their projection to the native space of each functional run. Frame-wise displacement (Power et al. 2014) was calculated for each functional run using the implementation of Nipype. ICA-based Automatic Removal Of Motion Artifacts (AROMA) was used to generate aggressive noise regressors as well as to create a variant of the data that is non-aggressively denoised (Pruim et al. 2015).

During the denoising stage, a confound regressor matrix was used to regress out confounding effects from the preprocessed RS-fMRI data, which included six head-motion parameters, the average signal within anatomically derived eroded WM mask, the average signal within anatomically derived eroded CSF mask, the average signal within the brain mask (Global), non-steady-state outliers (to remove outliers in the time series), and discrete cosine-basis regressors (to correct low-frequency signal drift). Finally, a 4th-order Butterworth low-pass temporal filter was applied, with a cutoff frequency of 0.2 Hz.

3 | Results

3.1 | Subjects With Greater Mean BOLD Intensity Have Greater amALFF and qmALFF but Not amfALFF or qmfALFF

At the subject level, MBI is calculated as the mean of MBI across all voxels within a given template in the brain. As shown in Figure 1a (China167) and Figure 1b (HCP1200), at the subject level, MBI positively correlates with amALFF in both the China167 ($p = 0.02$, $r = 0.18$) and HCP1200 ($p < 0.001$, $r = 0.91$) datasets. Similarly, MBI correlates with qmALFF (China167: $p = 0.02$, $r = 0.18$; HCP1200: $p < 0.001$, $r = 0.91$). These results underscore the necessity of normalizing amALFF and qmALFF by dividing them by their mean across all voxels within a specified mask to minimize inter-subject variability attributable to MBI and ensure comparability across subjects. The normalized amALFF and qmALFF are denoted as $\text{amALFF}_{\text{norm}}$ and $\text{qmALFF}_{\text{norm}}$, respectively, ensuring that their mean equals 1.

In contrast, MBI did not consistently scale with amfALFF (China167: $p = 0.51$, $r = 0.05$; HCP1200: low (l, pink): $p = 0.96$, $r = 0.02$; medium (m, green): $p = 0.14$, $r = 0.05$; high (h, blue): $p = 0.58$, $r = -0.05$) or qmfALFF (China167: $p = 0.43$, $r = 0.06$; HCP1200: low (l, pink): $p = 0.92$, $r = 0.03$; medium (m, green): $p = 0.18$, $r = 0.05$; high (h, blue): $p = 0.67$, $r = -0.04$).

3.2 | Across-Subject Relationships Between amALFF, qmALFF, amfALFF, and qmfALFF

As shown in Figure 1a (China167) and Figure 1b (HCP1200), qmALFF and amALFF exhibit a strong linear correlation, suggesting that qmALFF may behave approximately as a locally linear transformation of amALFF in both the China167 ($p < 0.001$, $r > 0.999$) and HCP1200 ($p < 0.001$, $r > 0.999$ across all clusters) datasets. Similarly, so too are qmfALFF and amfALFF (China167: $p < 0.001$, $r = 0.999$; HCP1200: $p < 0.001$, $r > 0.999$ across all clusters). When performing full-brain ALFF analyses across individuals, qm(f)ALFF and am(f)ALFF yield similar results.

Additionally, amALFF and amfALFF are positively correlated in both the China167 ($p < 0.001$, $r = 0.50$) and HCP1200 datasets

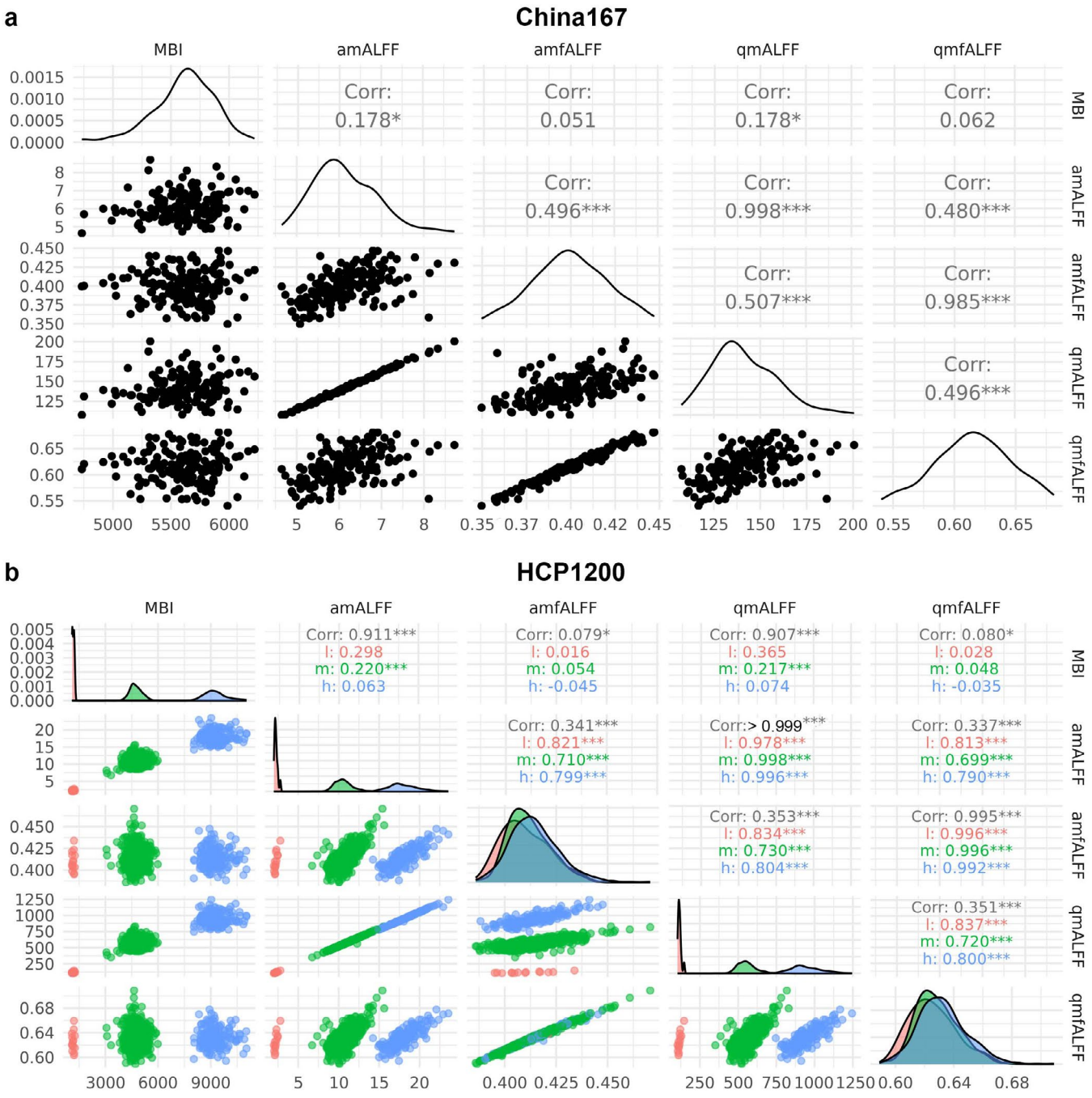

FIGURE 1 | Correlation matrix of mean BOLD intensity (MBI), amALFF, amfALFF, qmALFF, and qmfALFF for the China167 and HCP1200 datasets at the subject level. (a) For the China167 dataset, the MBI is weakly but significantly correlated with amALFF ($p=0.02$, $r=0.178$) and qmALFF ($p=0.02$, $r=0.178$) but not significantly correlated with amfALFF ($p=0.51$, $r=0.051$) or qmfALFF ($p=0.43$, $r=0.062$), Additionally, amALFF is significantly correlated with qmALFF ($p<0.001$, $r=0.998$), and amfALFF is significantly correlated with qmfALFF ($p<0.001$, $r=0.985$). The correlations between amALFF and amfALFF ($p<0.001$, $r=0.496$) and between qmALFF and qmfALFF ($p<0.001$, $r=0.496$) are significant. (b) Red, green, and blue colors represent 3 clusters with low (l), medium (m), and high (h) MBI value, respectively, for the HCP1200 dataset. As a whole, the MBI is significantly correlated with amALFF ($p<0.001$, $r=0.911$), qmALFF ($p<0.001$, $r=0.907$), amfALFF ($p=0.02$, $r=0.079$), and qmfALFF ($p=0.02$, $r=0.080$), Additionally, amALFF is significantly correlated with qmALFF ($p<0.001$, $r>0.999$), and amfALFF is significantly correlated with qmfALFF ($p<0.001$, $r=0.995$). The correlations between amALFF and amfALFF ($p<0.001$, $r=0.341$) and between qmALFF and qmfALFF ($p<0.001$, $r=0.351$) are significant. However, in the individual cluster, only the medium MBI cluster is significantly correlated with amALFF ($p<0.001$, $r=0.220$), and qmALFF ($p<0.001$, $r=0.217$). The correlations are greatly increased both between amALFF and amfALFF (l: 0.821, m: 0.710, and h: 0.799) and between qmALFF and qmfALFF (l: 0.837, m: 0.720, and h: 0.800).

(low (l, pink): $p<0.001$, $r=0.82$; medium (m, green): $p<0.001$, $r=0.71$; high (h, blue): $p<0.001$, $r=0.80$). A similar pattern is observed in the correlations between qmALFF and qmfALFF (China167: $p<0.001$, $r=0.51$ and HCP1200: low (l, pink): $p<0.001$, $r=0.83$; medium (m, green): $p<0.001$, $r=0.73$; high (h, blue): $p<0.001$, $r=0.80$).

3.3 | Mean BOLD Intensity Is Associated With amfALFF and qmfALFF but Not With amALFF$_{norm}$ or qmALFF$_{norm}$ at the Voxel Level

At the voxel level, the MBI is calculated as the mean of the MBIs across subjects for each voxel within a given template in a brain. As shown in Figure 2d (China167 with MNI152 brain mask) and Figure 2f (China167 with Schaefer mask), and Figure 2e (HCP1200 with MNI152 brain mask) and Figure 2g (HCP1200 with Schaefer mask), at the voxel level, MBI is moderately correlated with amfALFF in both the China167 ($p<0.001$, $r=0.23$; $p<0.001$, $r=0.25$) and HCP1200 ($p<0.001$, $r=0.21$; $p<0.001$, $r=0.26$) datasets for both masks. Similarly, MBI is significantly moderately correlated with qmfALFF (China167: $p<0.001$, $r=0.23$ and $p<0.001$, $r=0.26$; HCP1200: $p<0.001$, $r=0.22$ and $p<0.001$, $r=0.26$). However, MBI's correlation with the normalized metrics, amALFF$_{norm}$ or qmALFF$_{norm}$, is close to 0. At both the subject and the voxel levels, MBI was nearly orthogonal to the normalized ALFF metrics.

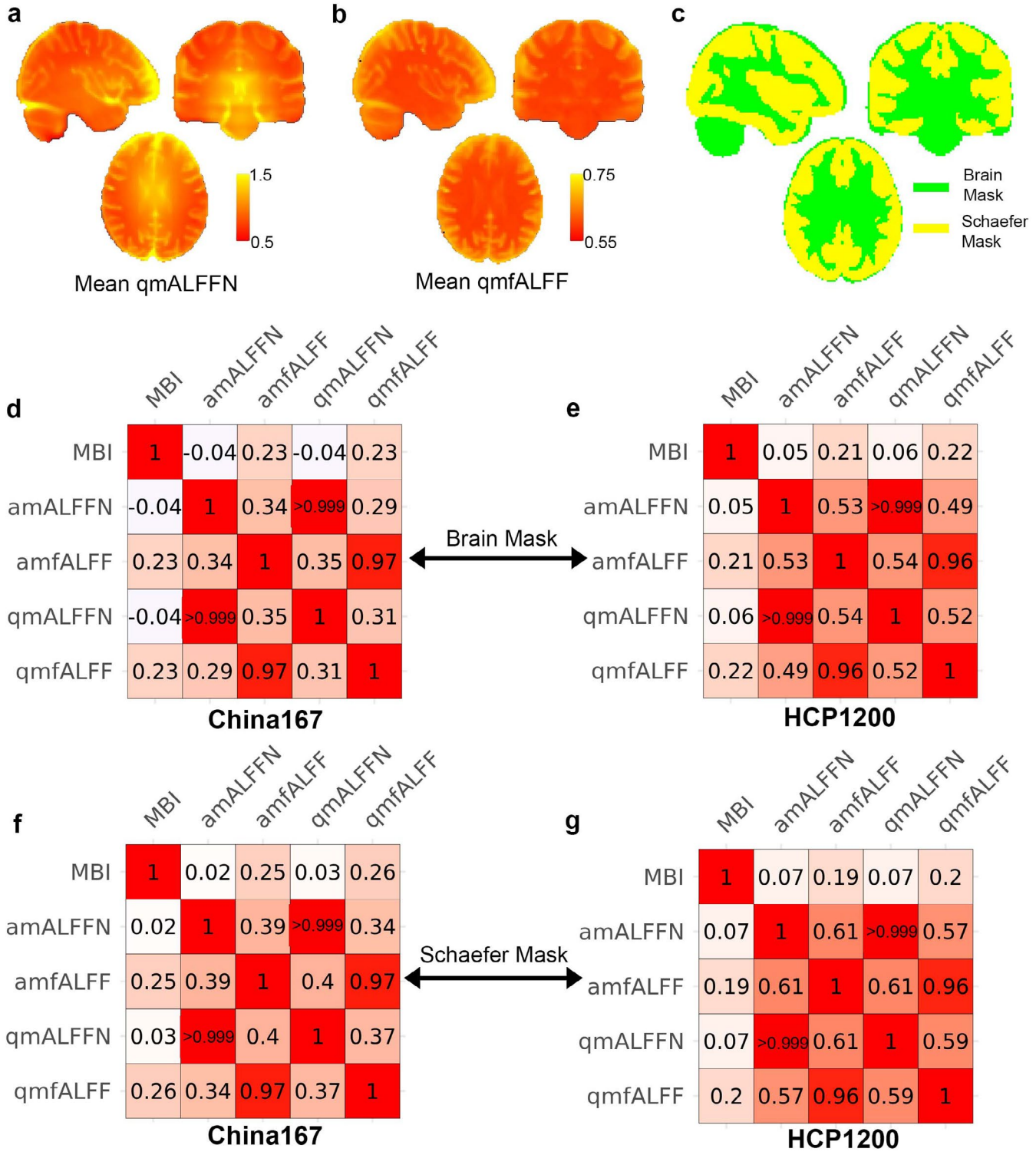

FIGURE 2 | Legend on next page.

FIGURE 2 | Correlation matrix of mean BOLD intensity (MBI), $amALFF_{norm}$, amfALFF, $qmALFF_{norm}$, and qmfALFF for the China167 and HCP1200 datasets at the voxel level. (a) and (b) Visualization of the mean $qmALFF_{norm}$ and $qmfALFF_{norm}$ across subject in the HCP1200 dataset. (c) Illustration of the MNI152 brain (green) and Schaefer (yellow) mask used in the analysis. (d) In the China167 dataset on the MNI152 brain mask, the MBI is significantly correlated with amfALFF ($p<0.001$, $r=0.23$) and qmfALFF ($p<0.001$, $r=0.23$), but shows no significant correlation with $amALFF_{norm}$ or $qmALFF_{norm}$. Notably, $amALFF_{norm}$ is highly significantly correlated with $qmALFF_{norm}$ ($p<0.001$, $r>0.999$), and amfALFF is significantly correlated with qmfALFF ($p<0.001$, $r=0.97$). Additionally, the relationships between $amALFF_{norm}$ and amfALFF ($p<0.001$, $r=0.34$), as well as between $qmALFF_{norm}$ and qmfALFF ($p<0.001$, $r=0.31$), show moderate but statistically significant correlations. (e) In the HCP1200 dataset on the MNI152 brain mask, the MBI is significantly correlated with amfALFF ($p<0.001$, $r=0.21$) and qmfALFF ($p<0.001$, $r=0.22$), but shows no significant correlation with $amALFF_{norm}$ or $qmALFF_{norm}$. Notably, $amALFF_{norm}$ is highly significantly correlated with $qmALFF_{norm}$ ($p<0.001$, $r>0.999$), and amfALFF is significantly correlated with qmfALFF ($p<0.001$, $r=0.96$). Additionally, the relationships between $amALFF_{norm}$ and amfALFF ($p<0.001$, $r=0.53$), as well as between $qmALFF_{norm}$ and qmfALFF ($p<0.001$, $r=0.52$), show moderate but statistically significant correlations. (f) In the China167 dataset on the Schaefer mask, the MBI is significantly correlated with amfALFF ($p<0.001$, $r=0.25$) and qmfALFF ($p<0.001$, $r=0.26$), but shows no significant correlation with $amALFF_{norm}$ or $qmALFF_{norm}$. Notably, $amALFF_{norm}$ is highly significantly correlated with $qmALFF_{norm}$ ($p<0.001$, $r>0.999$), and amfALFF is significantly correlated with qmfALFF ($p<0.001$, $r=0.97$). Additionally, the relationships between $amALFF_{norm}$ and amfALFF ($p<0.001$, $r=0.39$), as well as between $qmALFF_{norm}$ and qmfALFF ($p<0.001$, $r=0.37$), show moderate but statistically significant correlations. (g) In the HCP1200 dataset on the Schaefer mask, the MBI is significantly correlated with amfALFF ($p<0.001$, $r=0.19$) and qmfALFF ($p<0.001$, $r=0.20$), but shows no significant correlation with $amALFF_{norm}$ or $qmALFF_{norm}$. Notably, $amALFF_{norm}$ is highly significantly correlated with $qmALFF_{norm}$ ($p<0.001$, $r>0.999$), and amfALFF is significantly correlated with qmfALFF ($p<0.001$, $r=0.96$). Additionally, the relationships between $amALFF_{norm}$ and amfALFF ($p<0.001$, $r=0.61$), as well as between qmALFFN and qmfALFF ($p<0.001$, $r=0.59$), show moderate but statistically significant correlations.

3.4 | Relationships Among $amALFF_{norm}$, $qmALFF_{norm}$, amfALFF, and qmfALFF at the Voxel Level

As shown in Figure 2d (China167 with MNI152 brain mask), Figure 2f (China167 with Schaefer mask), Figure 2e (HCP1200 with MNI152 brain mask), and Figure 2g (HCP1200 with Schaefer mask), across voxels, $qmALFF_{norm}$ strongly correlated with $amALFF_{norm}$ across both datasets and masks (China167: $p<0.001$, $r>0.999$ for both masks; HCP1200: $p<0.001$, $r>0.999$ for MNI152 brain mask and $p<0.001$, $r=0.96$ for Schaefer mask). Similarly, qmfALFF strongly correlated with amfALFF (China167: $p<0.001$, $r=0.97$ for both masks; HCP1200: $p<0.001$, $r=0.97$ for both masks), indicating a strong relationship between the two variants of ALFF across voxels, as also observed across subjects.

Furthermore, across voxels, $amALFF_{norm}$ and amfALFF exhibit modest correlations in both China167 ($p<0.001$, $r=0.34$ for brain mask and $p<0.001$, $r=0.39$ for Schaefer mask) and HCP1200 datasets ($p<0.001$, $r=0.53$ for brain mask and $p<0.001$, $r=0.61$ for Schaefer mask). A similar pattern is observed in the correlations between $qmALFF_{norm}$ and qmfALFF (China167: $p<0.001$, $r=0.29$ for brain mask and $p<0.001$, $r=0.34$ for Schaefer mask, and HCP1200: $p<0.001$, $r=0.49$ for brain mask and $p<0.001$, $r=0.57$ for Schaefer mask). As shown in Figure 2a,b, correlations between $am(qm)ALFF_{norm}$ and am(qm)fALFF are consistently higher when using the Schaefer mask compared to the brain mask. This is likely due to the presence of elevated $am(qm)ALFF_{norm}$ values in white matter and vascular regions, which contribute to greater dissimilarity between the normalized and fractional metrics on the whole-brain mask.

3.5 | *Z*-Scoring Disrupts the Distribution of $qmALFF_{norm}$

From Equations (11) and (12), it is apparent that *z*-scoring the BOLD signal disrupts both $qmALFF_{norm}$ and $amALFF_{norm}$ across voxels, as the resulting $amALFF_{norm,z}$ and $qmALFF_{norm,z}$ become dependent on the standard deviation of the BOLD signal at each voxel, which varies across the brain. The extent of this disruption depends on the standard deviation of the BOLD signal at each voxel. Figure 3a,b illustrate the nonlinear relationship between $qmALFF_{norm}$ and $qmALFF_{z,norm}$, along with corresponding histograms of both metrics for the averaged China167 and HCP1200 datasets with Schaefer mask, respectively. In the China167 dataset, $qmALFF_{z,norm}$ explains only 4% of the variance in $qmALFF_{norm}$, whereas in the HCP1200 dataset, the shared variance is 28%. These findings indicate that z-scoring significantly alters the distribution of $qmALFF_{norm}$; thus, using the *z*-scored BOLD signal to compute ALFF is inappropriate.

3.6 | qmALFF Exhibits Higher Reliability Than qmfALFF and Both Perform Best at the Parcellation Level Compared to Voxel and Cortical Levels

As shown in Figure 4a (voxel level) and Figure 4b (parcellation level), $qmALFF_{norm}$ is strongly correlated with $amALFF_{norm}$ across subjects for both voxel (mean ± SD = 0.995 ± 0.001) and parcellation (mean ± SD = 0.9996 ± 0.0003) levels in the NU26 dataset. Similarly, qmfALFF shows strong correlation with amfALFF (voxel level: 0.936 ± 0.016; parcellation level: 0.988 ± 0.009). At the cortical level (Figure 4c and Figure 4d), mean qmALFF over Schaefer mask is highly correlated with mean amALFF ($r=0.999$, $p<0.001$) and mean qmfALFF is similarly correlated with mean amfALFF ($r=0.980$, $p<0.001$). These findings reconfirm a strong relationship between the two variants of ALFF across voxels, parcellation, and also across subjects.

Figure 4e–4h illustrate that qmALFF demonstrates higher reliability than qmfALFF at all levels: voxel (ICC mean ± SD: 0.499 ± 0.051 vs. 0.194 ± 0.065), parcellation (ICC mean ± SD: 0.871 ± 0.065 vs. 0.709 ± 0.186), and cortical (ICC mean: 0.795 vs. 0.297). Both qmALFF and qmfALFF achieve their best reliability at the parcellation level.

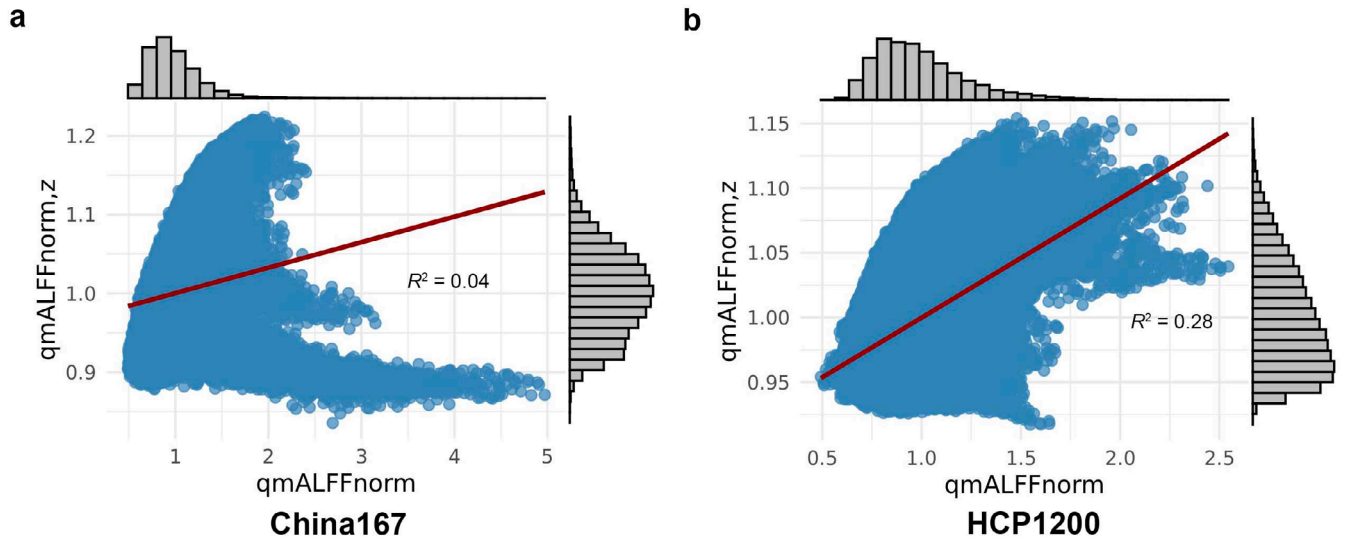

FIGURE 3 | Scatter plots illustrating the nonlinear relationship between $qmALFF_{norm}$ and $qmALFFZ_{norm,z}$, along with corresponding histograms of both metrics. (a) $R^2 = 0.04$ for China167 dataset with Schaefer mask; (b) $R^2 = 0.28$ for HCP1200 dataset with Schaefer mask.

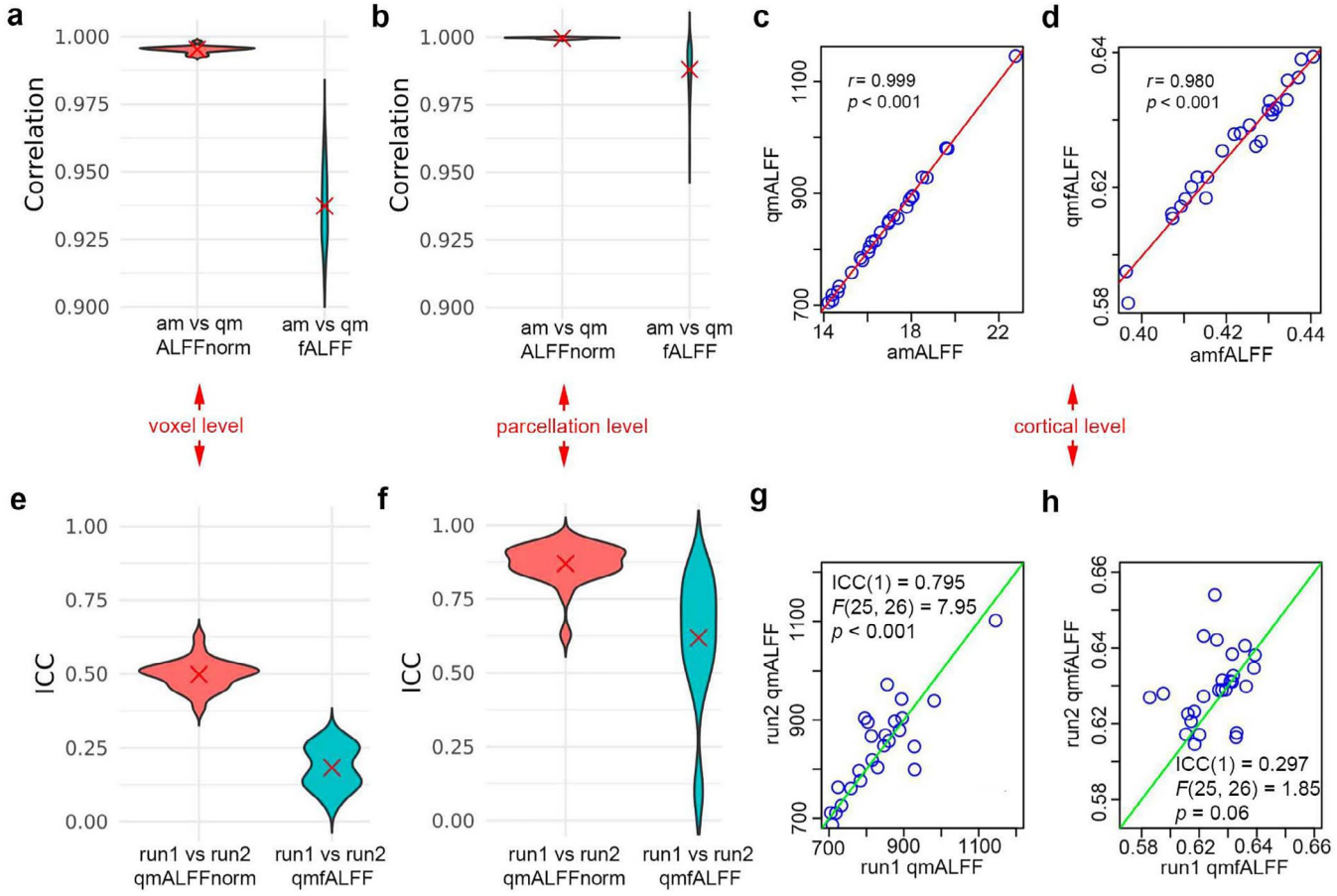

FIGURE 4 | Correlations between am(f)ALFF and qm(f)ALFF and reliability of qm(f)ALFF at voxel, parcellation, and cortical levels. (a) Violin plot of correlations between $amALFF_{norm}$ and $qmALFF_{norm}$ (left; mean ± SD = 0.995 ± 0.001) and between amfLAFF and qmfALFF (right; mean ± SD = 0.936 ± 0.016) at the voxel level. (b) Violin plot of correlations at parcellation level (left; mean ± SD = 0.9996 ± 0.0003; right; mean ± SD = 0.988 ± 0.009). (c, d) Scatter plots of correlations between am(f)ALFF and qm(f)ALFF at cortical level ($r = 0.999$, $p < 0.001$ and $r = 0.980$, $p < 0.001$). (e) Violin plot of ICC for $qmALFF_{norm}$ (left; mean ± SD = 0.499 ± 0.051) and qmfALFF (right; mean ± SD = 0.194 ± 0.065) at voxel level. (f) Violin plots of ICC at parcellation level (left; mean ± SD = 0.871 ± 0.065; right; mean ± SD = 0.709 ± 0.186). (g, h) ICC of qm(f)ALFF at cortical level (ICC(1) = 0.795, $p < 0.001$; and ICC = 0.297, $p = 0.06$). The red lines in panels **c** and **d** denote regression lines, whereas the green lines in panels **g** and **h** indicate the identity (diagonal) lines.

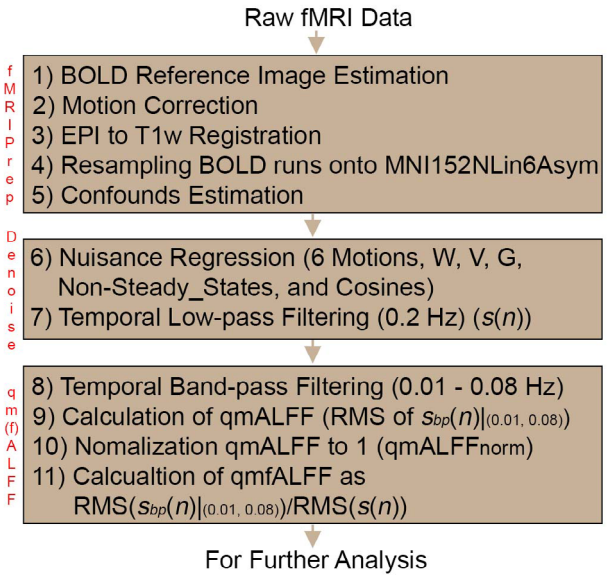

FIGURE 5 | Flowchart of calculating $qmALFF_{norm}$ and qmfALFF, starting from the preprocessing stage.

3.7 | Procedure for Calculating $qmALFF_{norm}$ and qmfALFF

Figure 5 illustrates the complete procedure for calculating $qmALFF_{norm}$ and qmfALFF, beginning with the preprocessing stage. The preprocessed RS-fMRI data is subjected to temporal band-pass filtering using a zero-lag fourth-order Butterworth filter with the frequency band of 0.01–0.08 Hz. Subsequently, qmALFF is calculated according to Equation (5) and $qmALFF_{norm}$ by normalizing qmALFF with its mean value. Simultaneously, qmfALFF is computed using Equation (6). All calculations are performed in the time domain, without applying an FFT. This procedure is implemented in R, and the corresponding script is available on https://github.com/lejianhuang/ALFF.

4 | Discussion

In this study, we clarified and resolved the inconsistencies in the definition and implementation of ALFF, and we introduced a novel variant called qmALFF. Our key findings include: (1) The mean BOLD intensity is strongly associated with both amALFF and qmALFF, necessitating normalization to their respective mean MBI across voxels; (2) $qmALFF_{norm}$ and qmfALFF are highly correlated with $amALFF_{norm}$ and amfALFF, respectively, at both subject and voxel levels; (3) z-scoring the BOLD signal does not affect amfALFF or qmfALFF, but it substantially alters both amALFF and qmALFF; (4) qmALFF exhibits higher reliability than qmfALFF and both perform best at the parcellation level compared to voxel and cortical levels.

The confusion surrounding the calculation of ALFF originates from the original publication by (Zang et al. 2007). The authors stated: "Since the power of a given frequency is proportional to the square of the amplitude of this frequency component [...], the square root was calculated at each frequency of the power spectrum and the averaged square root was obtained [...]. This averaged square root was taken as the ALFF" (Section 2.5. ALFF analysis in by (Zang et al. 2007)). They used the SPM software (Friston 2007) to compute the square of the amplitude at each frequency component, followed by averaging their square roots—an indirect and potentially misleading process for calculating the arithmetic mean of ALFF. This approach introduces ambiguity in the field, blurring the conceptual line between "amplitude" and "mean amplitude". More precisely, the mean amplitude of low-frequency fluctuation reflects changes in spontaneous neuronal activity. Although normalizing amALFF by its subject-level mean (i.e., computing $amALFF_{norm}$) effectively removes the effect of MBI and reduces inter-subject variability across individuals, it also masks the definitional inconsistency that persists in (Zuo et al. 2010)—namely, defining ALFF as the sum of amplitudes rather than the mean amplitude. This discrepancy becomes mathematically obscured because the factors in Equation (7) cancel out during normalization. Fortunately, our results demonstrate that these definitional inconsistencies do not compromise previous findings. Our data clearly show that $amALFF_{norm}$ and $qmALFF_{norm}$ are nearly perfectly correlated ($r \approx 1$) at voxel, parcellation, and cortical (subject) levels across three datasets and two different mask templates.

Our proposed qmALFF method, which derives from the concept of signal energy and its corresponding average power, provides a more physically grounded measure of mean amplitude in the frequency domain. In physics and engineering, the power or energy of a signal is proportional to the square of its amplitude—a principle to which qmALFF directly relates. Importantly, qmALFF can be computed either in the frequency domain (Equation (3)) or in the time domain (Equation (5)), making it flexible for implementation. Notably, the Conn toolbox (https://web.conn-toolbox.org/fmri-methods/connectivity-measures/other) (Whitfield-Gabrieli and Nieto-Castanon 2012) computes ALFF and fALFF using the time-domain formulation, but incorrectly cites references (Zang et al. 2007; Zou et al. 2008), which describe the original and potentially flawed definitions of ALFF and fALFF. Our work helps reconcile this inconsistency.

qmfALFF, like amfALFF, quantifies the relative contribution of low-frequency fluctuations within a given band to the whole frequency range determined by the cut-off frequencies in the preprocessing stage (Zou et al. 2008; Egorova et al. 2017). Although the correlation between qmfALFF and qmALFF is moderate ($r = 0.3–0.5$, see Figure 1), qmfALFF has a key advantage: it is insensitive to MBI at the subject level and unaffected by z-scoring of the BOLD. As such, it remains an essential measure for assessing the intensity of spontaneous neural activity within a specified frequency band. However, at the voxel level, qmfALFF shows a modest association with MBI ($r \approx 0.2$, see Figure 2). Addressing how to remove this voxel-level MBI effect in qmfALFF remains an open question for future work.

Several factors influence MBI. First, individual differences—such as variations in brain structure, vascularization, and metabolism—can lead to variability across subjects (Huang et al. 2012; Krishnamurthy et al. 2020). Second, physiological noise during scanning, including respiration, cardiac activity, and brain motion, which is strongly linked to respiration (Huang et al. 2024), can affect MBI measurements. Third, scanner settings play a significant role. Factors such as manufacturer, magnetic field

strength, echo time, repetition time, and flip angle all impact the MBI. In this study, the two datasets analyzed were acquired using scanners from different manufacturers, with identical magnetic field strengths but differing echo times, repetition times, and flip angles. Additionally, the scanner software version is another important variable. For instance, subjects in the HCP1200 dataset were scanned using the same brand of scanner with consistent parameters over 3 years (Ugurbil et al. 2013; Van Essen et al. 2013). However, as shown in Figure 1b, three distinct clusters of MBI values are observed. A plausible explanation is that the scanner software was updated three times during this period, potentially altering data resolution and applying GE's auto-scaling processes, which constrain the data range. Although the signal-to-noise ratio remained relatively stable, the MBI varied significantly, which in turn affected the am/qmALFF values. Therefore, normalizing am/qmALFF is essential to reduce inter-subject variability caused by these factors and to ensure comparability across individuals.

The quadratic mean is always greater than or equal to the arithmetic mean, making $qmALFF_{norm}$ more sensitive to larger deviations in time series compared to $amALFF_{norm}$. This property broadens the overall value range—values increase when $qmALFF_{norm}$ exceeds 1 and decrease when it falls between 0 and 1—thereby enhancing contrast among regions of interest (ROIs) within an individual brain. Consequently, as illustrated in Figure 2a, the quadratic mean decreases in cortical regions relative to the arithmetic mean, while increasing in white matter and ventricular regions. To further improve contrast within the cortex, rather than using the MNI152 brain as the normalization mask, we propose extracting each individual's gray matter from their anatomical T1 image and constructing a study-specific cortical template. This approach excludes white matter and cerebrospinal fluid, thereby enhancing contrast among cortical ROIs. In addition, qmfALFF demonstrates lower reliability than amALFF, particularly at the voxel level (mean ICC = 0.19; see Figure 4e). Spatial smoothing appears to improve reliability, as indicated by the increase in mean ICC to 0.71 at the parcellation level (Figure 4f). Therefore, both template-based normalization and spatial smoothing should be considered in future implementations within analysis toolboxes.

5 | Limitations

The use of multiple sites or centers in clinical trials and data-sharing initiatives to expand the subject pool has become a common practice. However, we observed that the distribution of am(qm)fALFF values, as shown in Figure 1, differs significantly between the two datasets analyzed. This discrepancy highlights the need to address site- and dataset-specific effects. To enable unbiased comparisons of ALFF or fALFF across different populations, it is essential to develop a robust framework that accounts for these inter-site and inter-dataset variations. In addition, the subject size for test–retest reliability analysis remains relatively small.

6 | Conclusions

In this study, we provided a mathematical clarification of ALFF and fALFF by introducing two novel variants: amALFF and qmALFF. Upon identifying an appreciable correlation between am(qm)ALFF and MBI, we emphasized the importance of normalizing these measures to subject-level means. Compared to amALFF, qmALFF offers the advantage of being computable directly in the time domain. To facilitate reproducibility and further research, we have implemented the complete procedure for calculating qm(f)ALFF in R. The corresponding script is publicly available at: https://github.com/lejianhuang/ALFF.

Author Contributions

All authors contributed substantially to this work. A.V.A. supervised the overall project. L.H. and R.H. conceived and designed the study and developed the methodology. L.H., R.H., and A.D.V. analyzed the data. A.D.V., P.B. and M.N.B. contributed to statistical modeling and interpretation of results. L.H. drafted the initial manuscript. A.D.V. and A.V.A. revised the manuscript. All authors reviewed, revised, and approved the final version of the manuscript.

Acknowledgments

We thank NIH (grant 1P50DA044121-01A1) for funding data analysis. This material is based upon work supported by the National Science Foundation Graduate Research Fellowship under grant no. DGE-1324585.

Funding

This work was supported by the National Institutes of Health (grant no. 1P50DA044121-01A1), National Science Foundation (grant no. DGE-1324585).

Conflicts of Interest

The authors declare no conflicts of interest.

Data Availability Statement

The data that support the findings of this study are openly available in github and openpain at https://github.com/lejianhuang/ALFF.

References

Avants, B. B., C. L. Epstein, M. Grossman, and J. C. Gee. 2008. "Symmetric Diffeomorphic Image Registration With Cross-Correlation: Evaluating Automated Labeling of Elderly and Neurodegenerative Brain." *Medical Image Analysis* 12, no. 1: 26–41.

Bartko, J. J. 1966. "The Intraclass Correlation Coefficient as a Measure of Reliability." *Psychological Reports* 19, no. 1: 3–11.

Behzadi, Y., K. Restom, J. Liau, and T. T. Liu. 2007. "A Component Based Noise Correction Method (CompCor) for BOLD and Perfusion Based fMRI." *NeuroImage* 37, no. 1: 90–101.

Biswal, B., F. Z. Yetkin, V. M. Haughton, and J. S. Hyde. 1995. "Functional Connectivity in the Motor Cortex of Resting Human Brain Using Echo-Planar MRI." *Magnetic Resonance in Medicine* 34, no. 4: 537–541.

Cattarinussi, G., F. Di Camillo, D. A. Grimaldi, and F. Sambataro. 2025. "Diagnostic Value of Regional Homogeneity and Fractional Amplitude of Low-Frequency Fluctuations in the Classification of Schizophrenia and Bipolar Disorders." *European Archives of Psychiatry and Clinical Neuroscience* 275, no. 3: 799–812.

Chang, X., Y. Yang, Y. Li, Z. Li, H. Zeng, and J. Su. 2025. "Gradient of White Matter Functional Variability via fALFF Differential

Identifiability." in *Proceedings of IEEE International Conference on Bioinformatics and Biomedicine (BIBM)*, 819–826.

Cordes, D., V. M. Haughton, K. Arfanakis, et al. 2001. "Frequencies Contributing to Functional Connectivity in the Cerebral Cortex in "Resting-State" Data." *AJNR. American Journal of Neuroradiology* 22, no. 7: 1326–1333.

Cox, R. W. 1996. "AFNI: Software for Analysis and Visualization of Functional Magnetic Resonance Neuroimages." *Computers and Biomedical Research* 29, no. 3: 162–173.

Dale, A. M., B. Fischl, and M. I. Sereno. 1999. "Cortical Surface-Based Analysis. I. Segmentation and Surface Reconstruction." *NeuroImage* 9, no. 2: 179–194.

Egorova, N., M. Veldsman, T. Cumming, and A. Brodtmann. 2017. "Fractional Amplitude of Low-Frequency Fluctuations (fALFF) in Post-Stroke Depression." *NeuroImage: Clinical* 16: 116–124.

Esteban, O., C. J. Markiewicz, R. W. Blair, et al. 2019. "fMRIPrep: A Robust Preprocessing Pipeline for Functional MRI." *Nature Methods* 16, no. 1: 111–116.

FCP-INDI, F.-I. F. C. P.-I. N. D.-s. I. 2024. *C-PAC (Clinical Connectivity Pipeline Analysis Connectivity), FCP-INDI*. Child Mind Institute.

Fonov, V. S., A. C. Evans, R. C. McKinstry, C. R. Almli, and D. L. Collins. 2009. "Unbiased Nonlinear Average Age-Appropriate Brain Templates From Birth to Adulthood." *NeuroImage* 47: S102.

Friston, K. J. 2007. *Statistical Parametric Mapping: The Analysis of Funtional Brain Images*. Elsevier/Academic Press.

Gorgolewski, K., C. D. Burns, C. Madison, et al. 2011. "Nipype: A Flexible, Lightweight and Extensible Neuroimaging Data Processing Framework in Python." *Frontiers in Neuroinformatics* 5: 13.

Gorgolewski, K. J., D. G. Ellis, M. P. Notter, et al. 2017. *Nipype: A Flexible, Lightweight and Extensible Neuroimaging Data Processing Framework in Python*. Frontiers Research Foundation.

Greve, D. N., and B. Fischl. 2009. "Accurate and Robust Brain Image Alignment Using Boundary-Based Registration." *NeuroImage* 48, no. 1: 63–72.

Handwerker, D. A., V. Roopchansingh, J. Gonzalez-Castillo, and P. A. Bandettini. 2012. "Periodic Changes in fMRI Connectivity." *NeuroImage* 63, no. 3: 1712–1719.

Huang, L., X. Wang, M. N. Baliki, L. Wang, A. V. Apkarian, and T. B. Parrish. 2012. "Reproducibility of Structural, Resting-State BOLD and DTI Data Between Identical Scanners." *PLoS One* 7, no. 10: e47684.

Huang, S., A. D. Vigotsky, A. V. Apkarian, and L. Huang. 2024. "Body Mass Index Associated With Respiration Predicts Motion in Resting-State Functional Magnetic Resonance Imaging Scans." *Human Brain Mapping* 45, no. 13: e70015.

Jenkinson, M., P. Bannister, M. Brady, and S. Smith. 2002. "Improved Optimization for the Robust and Accurate Linear Registration and Motion Correction of Brain Images." *NeuroImage* 17, no. 2: 825–841.

Jia, X. Z., J. Wang, H. Y. Sun, et al. 2019. "RESTplus: An Improved Toolkit for Resting-State Functional Magnetic Resonance Imaging Data Processing." *Science Bulletin (Beijing)* 64, no. 14: 953–954.

Klein, A., S. S. Ghosh, F. S. Bao, et al. 2017. "Mindboggling Morphometry of Human Brains." *PLoS Computational Biology* 13, no. 2: e1005350.

Krishnamurthy, V., L. C. Krishnamurthy, J. H. Drucker, et al. 2020. "Correcting Task fMRI Signals for Variability in Baseline CBF Improves BOLD-Behavior Relationships: A Feasibility Study in an Aging Model." *Frontiers in Neuroscience* 14: 336.

Lencz, T., A. Moyett, M. Argyelan, et al. 2022. "Frontal Lobe fALFF Measured From Resting-State fMRI as a Prognostic Biomarker in First-Episode Psychosis." *Neuropsychopharmacology* 47, no. 13: 2245–2251.

Li, T., Z. Liao, Y. Mao, et al. 2021. "Temporal Dynamic Changes of Intrinsic Brain Activity in Alzheimer's Disease and Mild Cognitive Impairment Patients: A Resting-State Functional Magnetic Resonance Imaging Study." *Annals of Translational Medicine* 9, no. 1: 63.

Liang, S., D. He, B. Qin, et al. 2025. "Frequency-Dependent Changes in Wavelet-ALFF in Patients With Acute Basal Ganglia Ischemic Stroke: A Resting-State fMRI Study." *Neural Plasticity* 2025: 8003718.

Liu, Y., Y. K. Hsien, W. Su, et al. 2025. "Frequency-Dependent Changes in the Amplitude of Low-Frequency Fluctuations in Post Stroke Apathy: A Resting-State fMRI Study." *Frontiers in Psychiatry* 16: 1458602.

Mieling, M., M. Gottlich, M. Yousuf, and N. Bunzeck. 2023. "Basal Forebrain Activity Predicts Functional Degeneration in the Entorhinal Cortex in Alzheimer's Disease." *Brain Communications* 5, no. 5: fcad262.

Mohanty, R., W. A. Sethares, V. A. Nair, and V. Prabhakaran. 2020. "Rethinking Measures of Functional Connectivity via Feature Extraction." *Scientific Reports* 10, no. 1: 1298.

Montalà-Flaquer, M., C. Cañete-Massé, L. Vaqué-Alcázar, D. Bartrés-Faz, M. Peró-Cebollero, and J. Guàrdia-Olmos. 2023. "Spontaneous Brain Activity in Healthy Aging: An Overview Through Fluctuations and Regional Homogeneity." *Frontiers in Aging Neuroscience* 14: 1002811.

Nieto-Castanon, A. 2020. *Handbook of Functional Connectivity Magnetic Resonance Imaging Methods in CONN*. Hilbert Press.

Power, J. D., A. Mitra, T. O. Laumann, A. Z. Snyder, B. L. Schlaggar, and S. E. Petersen. 2014. "Methods to Detect, Characterize, and Remove Motion Artifact in Resting State fMRI." *NeuroImage* 84: 320–341.

Pruim, R. H. R., M. Mennes, D. van Rooij, A. Llera, J. K. Buitelaar, and C. F. Beckmann. 2015. "ICA-AROMA: A Robust ICA-Based Strategy for Removing Motion Artifacts From fMRI Data." *NeuroImage* 112: 267–277.

Schaefer, A., R. Kong, E. M. Gordon, et al. 2018. "Local-Global Parcellation of the Human Cerebral Cortex From Intrinsic Functional Connectivity MRI." *Cerebral Cortex* 28, no. 9: 3095–3114.

Song, X. W., Z. Y. Dong, X. Y. Long, et al. 2011. "REST: A Toolkit for Resting-State Functional Magnetic Resonance Imaging Data Processing." *PLoS One* 6, no. 9: e25031.

Sun, J., C. Guo, Y. Ma, et al. 2022. "A Comparative Study of Amplitude of Low-Frequence Fluctuation of Resting-State fMRI Between the Younger and Older Treatment-Resistant Depression in Adults." *Frontiers in Neuroscience* 16: 949698.

Ugurbil, K., J. Xu, E. J. Auerbach, et al. 2013. "Pushing Spatial and Temporal Resolution for Functional and Diffusion MRI in the Human Connectome Project." *NeuroImage* 80: 80–104.

Van Essen, D. C., S. M. Smith, D. M. Barch, et al. 2013. "The WU-Minn Human Connectome Project: An Overview." *NeuroImage* 80: 62–79.

Whitfield-Gabrieli, S., and A. Nieto-Castanon. 2012. "Conn: A Functional Connectivity Toolbox for Correlated and Anticorrelated Brain Networks." *Brain Connectivity* 2, no. 3: 125–141.

Xu, K., Y. Liu, Y. Zhan, J. Ren, and T. Jiang. 2018. "BRANT: A Versatile and Extendable Resting-State fMRI Toolkit." *Frontiers in Neuroinformatics* 12: 52.

Yan, C. G., B. Cheung, C. Kelly, et al. 2013. "A Comprehensive Assessment of Regional Variation in the Impact of Head Micromovements on Functional Connectomics." *NeuroImage* 76: 183–201.

Yang, H., X. Y. Long, Y. H. Yang, et al. 2007. "Amplitude of Low Frequency Fluctuation Within Visual Areas Revealed by Resting-State Functional MRI." *NeuroImage* 36, no. 1: 144–152.

Yang, L., A. D. Vigotsky, B. Wu, et al. 2022. "Morphometric Similarity Networks Discriminate Patients With Lumbar Disc Herniation From Healthy Controls and Predict Pain Intensity." *Frontiers in Network Physiology* 2: 992662.

Yang, L., Y. Yan, Y. Wang, et al. 2018. "Gradual Disturbances of the Amplitude of Low-Frequency Fluctuations (ALFF) and Fractional ALFF in Alzheimer Spectrum." *Frontiers in Neuroscience* 12: 975.

Zang, Y. F., Y. He, C. Z. Zhu, et al. 2007. "Altered Baseline Brain Activity in Children With ADHD Revealed by Resting-State Functional MRI." *Brain & Development* 29, no. 2: 83–91.

Zhang, L., H. Yan, C. Zhang, et al. 2025. "The Application of Amplitude of Low-Frequency Fluctuations Metrics in the Diagnosis and Prediction of Treatment Response as Well as Their Associated Genes and Biological Processes in Patients With Bipolar Disorder." *Translational Psychiatry* 15, no. 1: 446.

Zhang, Y., M. Brady, and S. Smith. 2001. "Segmentation of Brain MR Images Through a Hidden Markov Random Field Model and the Expectation-Maximization Algorithm." *IEEE Transactions on Medical Imaging* 20, no. 1: 45–57.

Zou, Q. H., C. Z. Zhu, Y. Yang, et al. 2008. "An Improved Approach to Detection of Amplitude of Low-Frequency Fluctuation (ALFF) for Resting-State fMRI: Fractional ALFF." *Journal of Neuroscience Methods* 172, no. 1: 137–141.

Zuo, X. N., A. Di Martino, C. Kelly, et al. 2010. "The Oscillating Brain: Complex and Reliable." *NeuroImage* 49, no. 2: 1432–1445.